THRUST MEASUREMENTS OF THE RIT-10 THRUSTER WITH DLR'S NEW THRUST BALANCE

SPACE PROPULSION 2022
ESTORIL, PORTUGAL | 09 – 13 MAY 2022

Jens Schmidt [(1)], Jens Simon [(1,2)], Andreas Neumann [(1)]

[(1)] German Aerospace Center (DLR), Institute of Aerodynamics and Flow Technology, Department of Spacecraft, Göttingen, Germany, Email: jens.schmidt@dlr.de
[(2)] Heilbronn University of Applied Sciences, Daimlerstraße 35, 74653 Künzelsau

KEYWORDS: Electric Propulsion, Ground Testing, Diagnostics, Thrust Balances

ABSTRACT:

To study electric propulsion devices, accurate long-time measurements of the low thrust forces are necessary. For this purpose, a new, lightweight thrust balance has been established to be used at DLR's STG-ET facility – the **D**LR **E**lectric **P**ropulsion Thrust **B**alance (DEPB). To evaluate the performance of this thrust balance, it has been operated to perform measurements of the well-studied RIT 10 gridded-ion thruster. The new thrust balance and its performance are demonstrated and a first estimate on accuracy and long-term stability shall be given. While the setup has been fully manufactured and calibrated, a final test using an electric thruster is still necessary. To study the behavior of the thrust balance, the RIT-10 thruster is operated for extended intervals on the DEPB thrust balance. The long-term stability in terms of thermal drift, effects of the fluid and electric interface and effects of the vacuum and plasma environment onto the thrust balance are studied.

1. INTRODUCTION

Electric space propulsion is taking over more and more applications from chemical propulsion systems. Being common for attitude and station keeping, recent satellite missions also use electric thrusters for orbital maneuvers, e.g. from GTO to GEO.(Holste et al., 2020; Neumann, 2017) The main advantages of electric propulsion are their very high propellant economy and a good controllability. On the other hand, the absolute thrust values of electric thrusters are low compared to their mass and power consumption, and this requires quite long firing times (Neumann, 2017). This entails the need for long on-ground testing, which has to be done under adequate vacuum conditions. Furthermore, the diagnostics equipment needed for qualification of electric thrusters is quite different from chemical propulsion diagnostics. Thrust measurement is common for both technologies, but electric propulsion requires force measurement in a low range and with a high stability, due to the required long firing times. Therefore, the design and construction of an accurate thrust balance for electric propulsion is quite challenging. This is mainly driven by two constraints: very low thrust forces in the range of mN down to µN, depending on the type of thruster, need to be accurately measured whilst EP thrusters have a very low thrust-to-mass ratio, often below 1:1000. Thus, even a small error can reveal a very different system performance. Additionally, the thermal drift of the thrust balance needs to be controlled or mitigated, since most electric propulsion devices heat up due to thermal losses within their systems. Within a vacuum environment, thermal control is very challenging, since convection cannot be used as the major process of heat transfer and therefore the system has to be thermally stabilized either radiative or by heat conduction using cooling water or electrical heating. Water cooling, in turn, requires additional supply lines to the thruster which affect thrust measurements by temperature and position sensitive tension forces which can easily reach the

measurement range of mN. Dealing with these constraints makes thrust measurement a crucial diagnostics task. This work will focus on thrust balances as a basic equipment for investigating thrusters, and show the qualification of a newly developed thrust balance at DLR.

Figure 1. View of the STG-ET vacuum facility.

The STG-ET ("Simulationsanlage für Treibstrahlen Göttingen – Elektrische Triebwerke") facility of the German Aerospace Center (DLR) in Göttingen is one of the largest test facilities for electric propulsion worldwide(Neumann, 2017), in which the use of thrust balances is essential for commercial and scientific users of the facility. This section describes the capabilities of DLR's STG-ET facility, which has been built specifically for simulation of a space environment and to test electric propulsion systems. For electric propulsion development and testing a variety of diagnostic methods are required and integrated in the STG-ET facility (Neumann, 2017).
The STG-ET facility is shown in Figure 1 and consists of a large vacuum chamber with an inner diameter of 5 m and a length of 12.2 m. To create a rough vacuum, a pump stand is used, containing a rotating vane pump and a Roots pump. Fine vacuum is created using 6 Edwards turbomolecular pumps connected to a second, smaller set of vane/Roots roughing pumps, reaching a stand-by pressure in the order of 10^{-6} mbar. The pumping speed can be significantly increased by the use of 18 Oerlikon Leybold cryopumps reaching a stand-by pressure in the low 10^{-7} mbar range (Neumann et al., 2019). Pumping speeds for gas flow rates for argon, krypton, and xenon released into the chamber at room temperature are 276000 l/s for xenon, 360000 l/s for krypton, and 452000 l/s for argon. To shield the chamber walls from sputtering due to high energetic ions from propulsion, a water-cooled graphite target is installed at the rear end of the chamber and the chamber walls are partly protected with graphite sheets. As displayed in, the whole front-end lid of the chamber can be removed allowing easy access and installation of diagnostic equipment and thrusters. The vacuum chamber can operate continuously at low pressures for extended periods of time up to several weeks or months, giving a unique opportunity for long-duration testing of electric thrusters.

2. THEORY

Thrust balances can be separated by type into three major configurations: hanging pendulums, inverted pendulums and torsional pendulums. The configuration studied within this work is called a double inverted pendulum, consisting of two pendulums connected by a plate with a given stiffness and elasticity. For any pendulum, the deflection angle θ of a pendulum with mass m, pivot length L and moment of inertia $I \approx L^2 m$ can be described by a dampened oscillator as given by Eq. 1. In this

equation, k is the spring constant and c is the dampening constant, ω_n is the natural frequency of the system and ζ is the normalized damping coefficient as given by Eq. 2 and 3. (Polk et al., 2017)

$$\ddot{\Theta} + 2\zeta\omega_n\dot{\theta} + {\omega_n}^2\theta = F(t)L/I \qquad \text{Eq. 1}$$

$$\omega_n = \sqrt{\frac{k}{I}} \qquad \text{Eq.2}$$

$$\zeta = \frac{c}{2}\sqrt{\frac{1}{k\,I}} \qquad \text{Eq. 3}$$

Using this set of equations, the response of the thrust balance due to impulsive or permanent loads can be solved analytically, neglecting non-linear effects such as hysteresis, which is commonly reported for pendulum type thrust balance (Junge, 1964; Soares and Marques, 2021). The steady state solution is found by Eq. 4 for a given thrust force F_t and pivot length L_t.

$$\Theta_{ss} = \frac{F_t L_t}{I{\omega_n}^2} = \frac{F_t L_t}{k} \qquad \text{Eq.4}$$

For the damped system, the solution for deflection as a function of time is found by Eq. 5 for the underdamped system ($\zeta < 1$), the critically damped system ($\zeta = 1$) and the overdamped system ($\zeta > 1$).

$$\frac{\theta(t)}{\Theta_{ss}} = \begin{cases} 1 - e^{-\zeta\omega_n t}\left[cos(\omega_d t) + \frac{\zeta \cdot sin(\omega_d t)}{\sqrt{1-\zeta^2}}\right] & \zeta < 1 \\ 1 - exp(-\zeta\omega_n t)\cdot(1-\omega_n t) & \zeta = 1 \\ 1 + \frac{1}{2\sqrt{\zeta^2-1}}\left[\frac{e^{-d_1\omega_n t}}{d_1} - \frac{e^{-d_2\omega_n t}}{d_2}\right] & \zeta > 1 \end{cases} \qquad \text{Eq.5}$$

The time to reach the steady-state deflection is governed by the damping coefficient. For thrust balances, multiple performance metrics are important: Sensitivity, Repeatability and Stability, Accuracy, Resolution, Noise, Response Time and Predictability of the Response. To gain information on these parameters, experimental verification is needed.

3. THRUST BALANCES AT DLR

At DLR, currently three thrust balances are available. Besides the thrust balance described within this work, two thrust balances have been developed in partnership with the company AST. The small (Neumann, 2017) and large balance have been sufficiently described within previous work (Neumann et al., 2021), but some limitations have been found during operation. These include the high sensitivity of the leaf spring bearings to loads as well as a challenging thermal control due to the high system mass.

To advance the ability to accurately measure thrust, a new thrust balance has been developed. This thrust balance, as shown in Figure 2, consists of an aluminium table, casing and 8 quartz-glass rods used as flexible bearings for the thruster table. Not displayed are the side panel with copper piping used for thermal regulation of the thrust balance. The thruster under test can be mounted on a removable table connected with the moving table of the balance by three form-fit connections. The force measurement and regulation of the balance in place is provided by a Sartorius® WZA224 load cell. High frequency oscillations are dampened by an eddy current brake, also not shown. The connection between the moving thrust balance table and the load cell is established by a micrometer-screw or either a high-precision motorized actuator. For this work, the micrometer-screw was used. The quartz rods were used due to the lower thermal expansion coefficient ($\alpha_{\parallel} = 0.59 \cdot 10^{-6} K^{-1}$) of quartz glass or compared to steel or aluminium ($\alpha_{\parallel} = 23.1 \cdot 10^{-6} K^{-1}$) resulting in a lower thermal drift of the balance (Neumann and Dahm, n.d.).

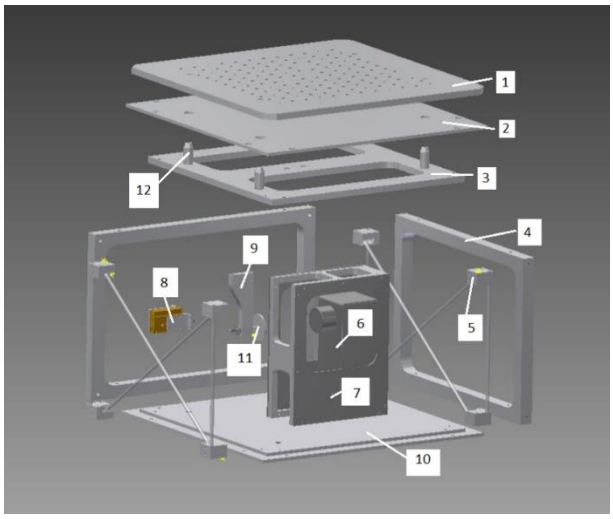

Figure 2. Assembly sketch of the main components of the thrust balance. The eddy current brake and side casing plates are not shown here. Parts: 1 thruster platform; 2 housing top plate; 3 upper moving platform; 4 housing frame; 5 flexible bearing rod assembly; 6 weigh cell; 7 weigh cell supporting frame; 8 calibration stage assembly; 9 Force transmission piece with screw; 10 base plate; 11 contact piece; 12 connection stud to thruster platform.

For the system under consideration, the spring constant is the sum of the individual spring constants of the system as calculated by Eq. 6.

$$k = \sum k_i = 4\frac{3\,E\,I}{{l_1}^3} + 4\frac{3\,E\,I}{{l_2}^3} \quad \text{Eq. 6}$$

In which $E = 7.25 \cdot 10^4 \frac{N}{mm^2}$ and $I = I_y = \frac{\pi d^4}{64} = 30.68\,mm^4$ are Young's modulus and the moment of inertia of the quartz glass rods with lengths l_1 and l_2. This results in a spring constant of $k \approx 3.54\,N/m$ for the system, if the unknown stiffness of connectors and feedlines is not included. The connector between balance table and load cell is assumed to not be flexible. If the inertia of the system is approximated with $I \approx {L_t}^2 m_t$, the frequency of the first normal mode is $\omega_n \approx 5.314\,s^{-1}$. The damping coefficient of the thrust balance has been experimentally determined to $\zeta \approx 0.25$.

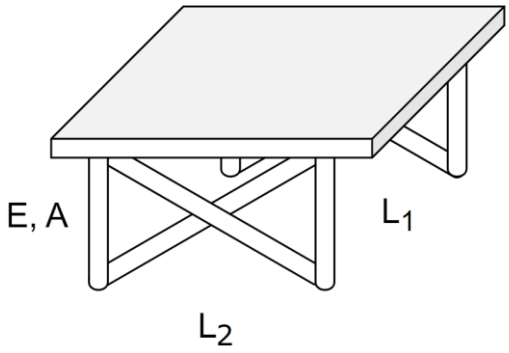

Figure 3: Figure of the relevant lengths of the mechanical system

4. EXPERIMENTAL SETUP

For calibration of the thrust balance, two methods have been set up. A calibrated load spring can be used to apply a force onto the table and is described in (Neumann et al., 2021). Additionally, a set of 3 fine weights has been attached onto the table of the thrust balance over a pulley and a Kevlar® thread. As displayed in *Figure 4*, a different amount of weights can be placed in the hanging position to change the load onto the cell by using a moveable plate. The exact mass of the weights and thread

have been determined using a high precision Sartorius scale with an uncertainty of $\Delta m = \pm 0.0001$ grams and is given in Table 1.

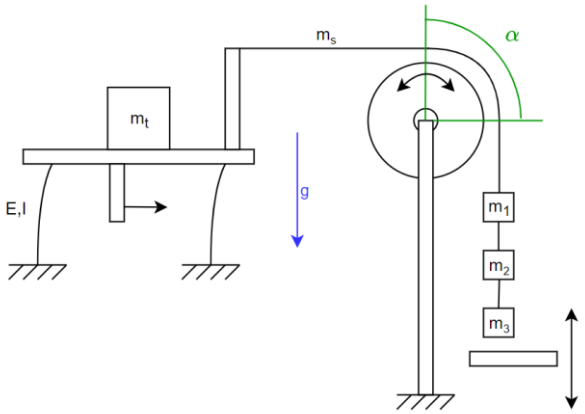

Figure 4: Calibration setup for the thrust balance with balance, pulley, 3 fine weights and moveable table. Not to scale.

Due to the pulley, not all force F_g is transmitted from the weights to the thrust balance. The balance of forces is given in Eq. 7 with $\mu = 0.16$ as the friction coefficient and $\alpha = \frac{\pi}{2}$ being the angle of the rope around the pulley resulting in a force $F = 0.9605 \cdot F_g$ on the thrust balance for a pulley with large radius R and small radius r.

$$F_g = F + \mu \frac{r}{R}(F + F_g)\sin(\frac{\alpha}{2}) \qquad \text{Eq. 7}$$

The known mass and therefore gravitational force of the calibration weights was then compared with the measured force of the load cell to calculate the calibration curve.

Table 1: Mass of the used calibration weights.

Mass	**Weight [g]**
m_1	0.3354
m_2	0.3427
m_3	0.3457
m_s	0.0072
m_{tot}	1.0382

For the qualification of the thrust balance, two distinct setups have been used within the MT vacuum chamber at DLR Göttingen, which has a length of 2m and a diameter of 1m. The vacuum pumps consist of a set of a *Leybold Varovac S100F* rotary vane, a *Leybold Ruvac WA501* Roots pump and a *Pfeiffer TPH2200* turbomolecular pump allowing for a minimum pressure of 3E-6 mbar. When a gas flow is introduced within the chamber, the pressure increases as a function of volume flow.
The first setup consists of a cold gas thruster operated with air fed from a reservoir at atmospheric pressure. This setup, as shown in Figure 5, was chosen to reduce the number of variables that influence the measurement. Besides the thrust balance bearings, the PTFE gas feed line and power lines to the valve are the only connections between the thruster on the balance and the chamber. The cold gas thruster has a nominal thrust of $F = 42.5\,mN$ with a specific impulse of $I_s = 64\,s$ with nitrogen and a reservoir pressure of $p_0 = 1.5\,bar$. With air at an ambient pressure $p_0 = 102584\,Pa$, the specific impulse reduces to $I_s = 43.6\,s$ and the thrust to $F = 26.2\,mN$. The thrust can also be further throttled by operating the valve at a lower voltage.

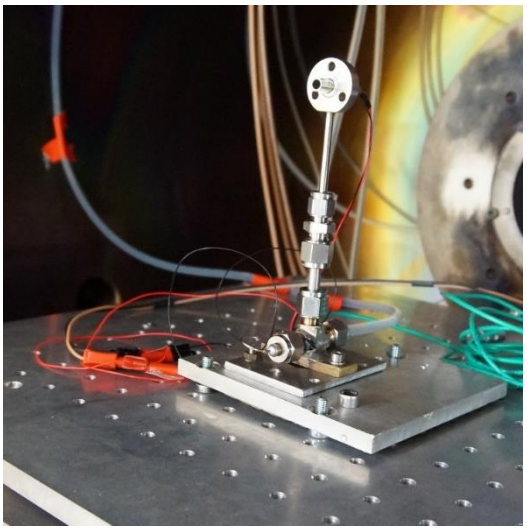

Figure 5: Thrust balance with cold gas thruster and gas connection on the thrust balance table

To qualify the balance for electric propulsion, a RIT-10 ion source including the radio frequency generator was set up on the thrust balance as shown in Figure 6. The RIT-10/37 thruster was set up with a 37-hole reduced grid. The radio frequency generator (RFG) was also positioned on the thrust balance. For operation of the ion source, several feed lines were connected to the thruster. The feedlines include a PTFE gas feedline, two silicone water lines for cooling of the thruster and RFG, three high voltage connectors for the grids, power supply to the RFG and two cables for the temperature sensors within the source. Due to this rather complex setup, the connected feed and power lines might have a large influence on the dynamic behaviour of the thrust balance. To protect the electronics and thruster from reflected ions from the chamber wall, graphite plates were placed around the thruster exit. Additionally, parts of the balance including the load cell were shielded with multi-layer-insulation (MLI) foil to minimize the thermal drift of the balance during operation of the thruster, since parts of the thruster can heat up to temperatures of 150°C and transfer the heat by radiation and conductivity to the sensitive components like the bearing, the load cell and the connector between balance table and load cell. For the operation with the RIT-10/37, the housing of the thrust balance has been used. Both thrusters were operated with the calibration mechanism described previously.

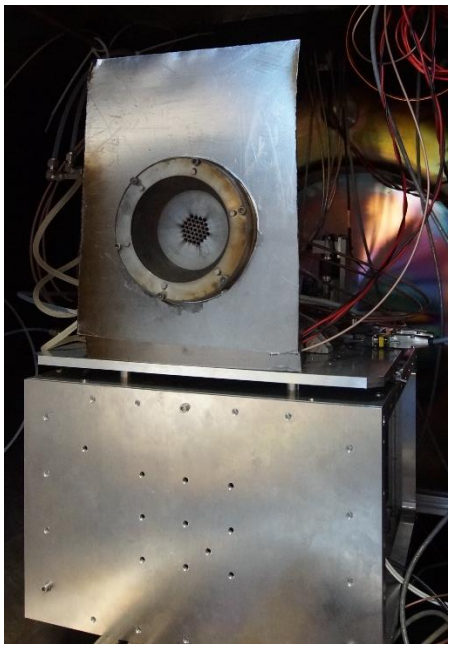

Figure 6: Thrust Balance with closed front plate and RIT-10 ion source.

5. RESULTS

The results can be separated into the results of the calibration, the cold gas thruster and the measurements with the radio frequency ion thruster.

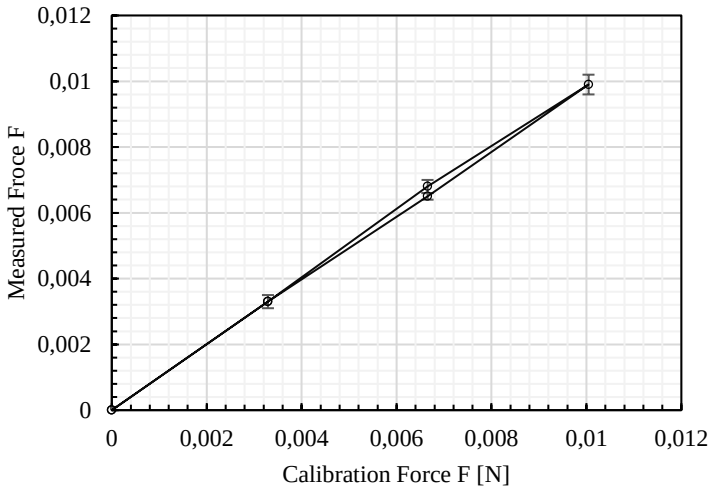

Figure 7: Calibration Curve of the thrust Balance with the RIT-10/37 thruster. Error bars show standard deviation over 5 measurements.

For the calibration, the load was applied and the measured force was compared after drift subtraction. The calibration process was conducted under atmosphere and under vacuum conditions at a pressure of $p = 5 \cdot 10^{-5}\, mbar$. It was observed, that the agreement between calibration force and measured force were better under vacuum. This is possibly due to the influence of the residual atmosphere on the weights and fiber. The calibration process was repeated multiple times before and after the thrust measurement. In Figure 7, the calibration curve of the thrust balance with the 3 fine weights is shown

as an average of 5 measurements. The drift and influence of the pulley were subtracted as discussed before. It can be seen, that for the middle weight, the value for increasing weights is higher than for decreasing weights. This is likely a hysteresis effect (Junge, 1964; Soares and Marques, 2021) of the balance and has to be studied more detailed in the future. Still, the deviation is within 3% of the calibration force. Overall, the influence of the cables of the feed lines on the thrust balance is relatively small, also within $\Delta F \approx \pm 3\%$.

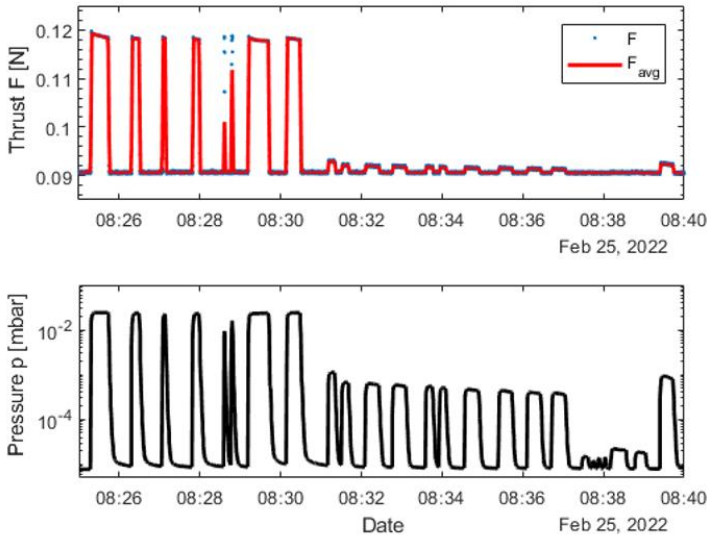

Figure 8: Measured force of the thrust balance and chamber pressure as a response to a cold gas thruster at nominal and throttled gas flow.

In Figure 8, the measured thrust and corresponding background pressure of the vacuum chamber are shown for the operation with the cold gas thruster with a reservoir at atmospheric pressure as described in the previous section. It can be seen, that when the valve of the thruster is opened, an initial thrust of $F \approx 28.5\, mN$ can be measured that decreases slightly over an extended period of operation. This decrease can be accounted to a change in thruster temperature due to the heating of the valve at continued operation and the cooling of the nozzle exit due to the expanding cold gas, for which an exit temperature of $T_e \approx 208\, K$ can be found analytically.
It can be seen that for the cold gas thruster, the measurement could be repeated several times with a constant thrust. Additionally, in Figure 8 also the operation with the throttled valve is shown and it can be shown, that the thrust reduces to $F \approx 1.4\, mN$. During operation of the turbomolecular pump, an oscillation of the measurement with a frequency of $f = 1.53\, Hz$ was observed.

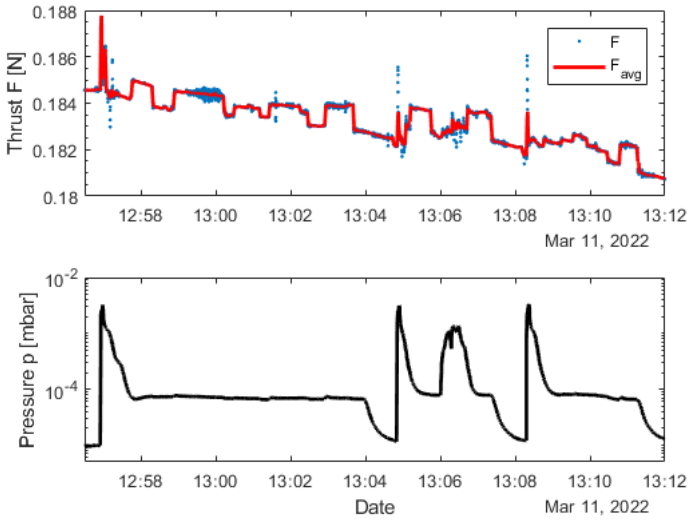

Figure 9: Measured force of the thrust balance and chamber pressure as a response to the RIT-10/37 ion source.

In Figure 9, the result of the thrust measurement with the RIT-10/37 are shown. The peaks in pressure are a result of the ignition of the thruster using a neutral gas shock. After the initial peak, mass flow and pressure stay constant. The used set points of the thruster are given in Table 2. A constant drift can be observed during operation due to the heat from the thruster discharge chamber leading to thermal stresses within the thrust balance structure.

Table 2: Operational setpoints of the RIT-10/37 thruster used for thrust measurements

	PHV [V]	**NHV [V]**	$\dot{V}$ **[sccm]**	P_{RF} **[W]**
#1	600	130	1	60.32
#2	1000	130	1	61.82
#3	1500	140	1	64.06
#4	2000	400	1	66.32

The large changes in measured thrust can therefore be attributed to changes in discharge conditions and acceleration voltage. After subtraction of the thermal drift, multiple measurements of the thrust can be averaged. The results are displayed in Figure 10. It can be seen, that the thrust increases with the acceleration voltage, if the mass flow and RF power are kept constant. For an acceleration grid bias of $U = -600\,V$, an average thrust of $F = 0.36\,mN$ was measured, while for the (maximum) voltage of $U = -2000\,V$, a thrust of $F = 1.2\,mN$ was measured. The RF frequency was $f_{RF} \approx 1.95\,MHz$. Therefore, the thrust balance was successfully operated with an electric thruster. The oscillation introduced by the turbomolecular pump was also observed with the gridded ion thruster on the thrust balance.

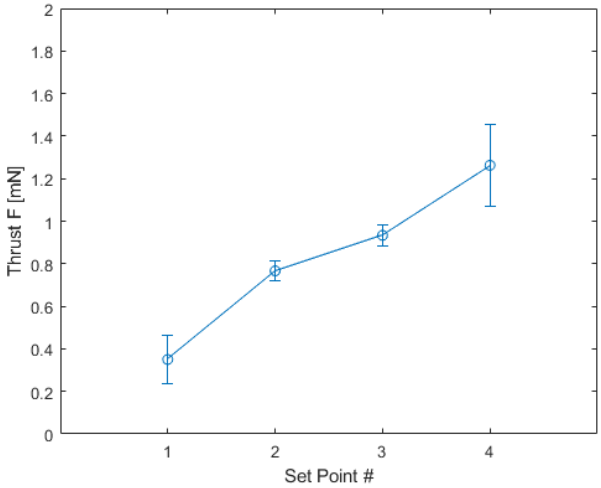

Figure 10: Measured thrust for the different setpoints given in Table 2. The bars depict the standard deviation.

6. DISCUSSION

Measurements were conducted with a cold gas thruster and gridded ion source. For the cold gas thruster, the measured thrust $F = 28.5\,mN$ was close to the estimated thrust $F = 26.2\,mN$ for the operation with air. The same value could be measured repeatedly and without any observed drift of the balance while having a fast response to the actuation of the valve. For cold gas thrusters reliable measurements can be conducted with this thrust balance.

With the gridded ion source, low thrust forces were measured. These correspond to measurements of the same ion source conducted with other thrust balances at DLR (Neumann et al., 2017). The thrust balance responds to different accelerating biases by a change in thrust measurement. When the acceleration bias is increased, the thrust increases. During the measurement with the ion thruster, a relatively slow, but significant drift was observed. This drift is caused by the thermal gradient within the vacuum chamber due to the hot thruster. It might be lowered by a better thermal control system and a larger vacuum chamber. The thrust balance itself also has a daily drift due to temperature change of the environment.

It was observed during the measurements with both thrusters, that the turbomolecular pump introduces a vibrational force on the thrust balance. This value is close to the first normal mode of the system. The difference to the calculated value can be attributed to the stiffness of the connected cables and the additional mass of the thrusters.

7. CONCLUSION

A new thrust balance has been qualified for thrust measurements at very low thrust levels with high accuracy over a wide range. Due to the use of quartz glass rods as bearings, even thrusters with a high mass-to-thrust ratio can be used. For qualification, a cold gas thruster has been used for simplicity of operation and to create a relatively high thrust. A RIT-10/37 ion source has been used to determine the response of the thrust balance to low forces. With the cold gas thruster, a thrust of $F = 28.5\,mN$ could be measured and with the ion source, different thrust levels in between $F = 0.2 - 1.4\,mN$ could be measured. The resolution of the thrust balance has been determined to be 0.2 mN, offering even the possibility to measure sub-mN thrusters. The noise level of the balance without pumps was in the range of $\Delta F \approx \pm 10^{-5} mN$ and can also be partially attributed to external noise from surrounding facilities. Still, the balance has still some options for future improvements. To keep the thrust balance thermally stable, a system for temperature control by heating shall be established. Additionally, the transfer of power can be optimized to reduce the stiffness of the installed cables. Low frequency oscillations which were observed but negligible for steady-state thrust measurements can be dampened in future setups.

8. REFERENCES

Holste, K., Dietz, P., Scharmann, S., Keil, K., Henning, T., Zschätzsch, D., Reitemeyer, M., Nauschütt, B., Kiefer, F., Kunze, F., Zorn, J., Heiliger, C., Joshi, N., Probst, U., Thüringer, R., Volkmar, C., Packan, D., Peterschmitt, S., Brinkmann, K.-T., Zaunick, H.-G., Thoma, M.H., Kretschmer, M., Leiter, H.J., Schippers, S., Hannemann, K., Klar, P.J., 2020. Ion thrusters for electric propulsion: Scientific issues developing a niche technology into a game changer. Rev. Sci. Instrum. 91, 061101. https://doi.org/10.1063/5.0010134

Junge, H., 1964. Untersuchungen über eine Feinschubmeßanlage für kontinuierliche elektrische Antriebe (Forschungsbericht No. DLR-FB 64-50). DFL, Braunschweig.

Neumann, A., 2017. STG-ET: DLR electric propulsion test facility. J. Large-Scale Res. Facil. JLSRF 3, 108. https://doi.org/10.17815/jlsrf-3-156

Neumann, A., Dahm, P., n.d. Schubwaage zum Messen von Schubkräften von elektrischen Raumfahrtantrieben. DE 10 2017 100 876 B4.

Neumann, A., Hannemann, K., Brchnelova, M., 2019. Challenges of Cryopumping EP-Propellants in DLR's Electric Propulsion Test Facility. Presented at the The 36th International Electric Propulsion Conference, Vienna, Austria.

Neumann, A., Simon, J., Schmidt, J., 2021. Thrust measurement and thrust balance development at DLR's electric propulsion test facility. EPJ Tech. Instrum. 8, 1–19. https://doi.org/10.1140/epjti/s40485-021-00074-7

Neumann, A., Volkmar, C., Geile, C., Hannemann, K., 2017. Mitigation of Detrimental Electric Thruster Force Measurement Effects. Presented at the 35th International Electric Propulsion Conference, Atlanta, Georgia, USA.

Polk, J.E., Pancotti, A., Haag, T., King, S., Walker, M., Blakely, J., Ziemer, J., 2017. Recommended Practice for Thrust Measurement in Electric Propulsion Testing. J. Propuls. Power 33, 539–555. https://doi.org/10.2514/1.B35564

Soares, D.L.O., Marques, R.I., 2021. In vacuum dynamic and static tests of a thrust balance for electric propulsion with hysteresis analysis and behaviour prediction with transfer function. Meas. Sci. Technol. 32, 125903. https://doi.org/10.1088/1361-6501/ac271d